Carbohydrate Polymers 175 (2017) 18–26

Contents lists available at ScienceDirect

Carbohydrate Polymers

journal homepage: www.elsevier.com/locate/carbpol

Chiroplasmonic magnetic gold nanocomposites produced by one-step aqueous method using κ-carrageenan

Marina V. Lesnichaya[a,*], Boris G. Sukhov[a], Galina P. Aleksandrova[a], Ekaterina R. Gasilova[b], Tamara I. Vakul'skaya[a], Spartak S. Khutsishvili[a], Anatoliy N. Sapozhnikov[c], Igor V. Klimenkov[d], Boris A. Trofimov[a]

[a] A.E. Favorsky Irkutsk Institute of Chemistry, Siberian Branch, Russian Academy of Sciences, 1, Favorsky St., 664033, Irkutsk, Russia
[b] Institute of Macromolecular Compounds, Russian Academy of Sciences, 31, Bolshoy pr., 199004, Saint-Petersburg, Russia
[c] A.P. Vinogradov Institute of Geochemistry, Siberian Branch, Russian Academy of Sciences, 1a, Favorsky St., 664033, Irkutsk, Russia
[d] Limnological Institute, Siberian Branch, Russian Academy of Sciences, 3, Ulan-Batorskaya St., 664033, Irkutsk, Russia

ARTICLE INFO

Article history:
Received 13 November 2016
Received in revised form 12 July 2017
Accepted 13 July 2017
Available online 18 July 2017

Chemical compounds studied in this article:
Carrageenan- kappa PubChem CID: 11966249
Sodium hydroxide PubChem CID: 14798
Chlorauric acid PubChem CID: 28133

Keywords:
κ-carrageenan
Gold nanoparticles
Cotton effect
Chiroplasmonic and magnetic properties

ABSTRACT

Novel water-soluble chiroplasmonic nanobiocomposites with directly varied gold content were synthesized by a one-step redox method in water using a biocompatible polysaccharide κ-carrageenan (industrial product from algae) as both reducing and stabilizing matrix. The influence of the reactants ratio, temperature, and pH on the reaction was studied and the optimal reaction parameters were found. The structure and the properties of composite nanomaterials were examined in solid state and aqueous solutions by using complementary physical-chemical methods X-ray diffraction analysis, transmission electron microscopy, spectroscopy of electron paramagnetic resonance, atomic absorption and optical spectroscopy, polarimetry including optical rotatory dispersion with registration of interphase-crossbred Cotton effect of a chiral polysaccharide matrix on plasmonic chromophore of gold nanoparticles, dynamic and static light scattering. The new perspective multi-purpose nanocomposites demonstrate a complex of chiroplasmonic and magnetic properties, imparted by both nanoparticles and radicals enriched chiral polysaccharide matrix.

1. Introduction

Because of unique size-depended set of physical, chemical, and biological properties of gold nanoparticles (AuNPs), they represent nowadays almost indispensable objects of research and application in diverse and ever developing areas of science and engineering. In particular, AuNPs are most intensively applied in biomedicine (Yamada, Foote & Prow, 2015), catalysis including its asymmetric (Yasukawa, Miyamura & Kobayashi, 2014) and plasmon-enhanced types (Kale, Avanesian & Christopher, 2014), plasmonics and related fields including "giant" surface-enhanced spectroscopy kinds (Lan & Wang, 2016) and the newest chiroplasmonic phenomena (Kuzyk et al., 2012; Kim et al., 2016). Apart from widely exploited size-dependent effects, AuNPs materials posses such essential properties as general operating safety, biocompatibility and controlled solubility in physiological fluids especially important for biomedicine. Moreover, the modern methods for the synthesis of AuNPs materials should be maximally eco-friendly.

Among existing methods for the chemical synthesis of AuNPs, the most widespread are those based on reduction of gold-containing precursors in aqueous solutions in the presence of reducing and stabilizing agents of AuNPs (Zhao, Li & Astruc, 2013). At that the most eco-friendly approach are which based on the use for the synthesis of AuNPs of various natural compounds. So, native plant juices and extracts microorganisms with their cultural and metabolic media, etc. contain in their composition reducing and nanostabilizing compounds for the AuNPs synthesis. (Mittal, Chisti & Banejee, 2013; Noruzi, 2015). However, a disadvantage of their application is variation of the biological composition depending on method for their preparation as well as on the region and the season of their collection and the type of vegetable raw material (or microorganism's types, their physiological phases and cultural media). This potentially hinders

* Corresponding author.
E-mail addresses: mlesnichaya@mail.ru, mlesnichaya@irioch.irk.ru (M.V. Lesnichaya).

http://dx.doi.org/10.1016/j.carbpol.2017.07.040
0144-8617/

the hard standardization of target gold-containing nanomaterials (moreover, it is generally unacceptable for most strict biomedical applications). The demand of environmental safety and absence of additional reducing reactants requires the application of readily available standardized biopolymers for AuNPs synthesis. For example, diverse plant polysaccharides acting as both reducing agents and nanoparticle stabilizers can be applied (Marradi, Chiodo, García, & Penadés, 2013; Trofimov et al., 2003; Zheng, Monty, & Linhardt, 2015). As a result, a spectrum of functional properties of polysaccharide-based nanomaterials is essentially expanded due to synergetic supplementation of effects of nanoparticles and various physical-chemical and biological properties of specific polysaccharide matrixes (Shurygina et al., 2011; Trofimov et al., 2003). From this point of view, one of the most attractive of polysaccharides for the AuNPs synthesis can act κ-carrageenan (κ-CG) – a biocompatible water-soluble sulfated polysaccharide extracted from red seaweed algae. It is one of the most promising available biopolymer. It is produced in large industrial scale and is widely used in the food industry and cosmetics (Prajapati, Maheriya, Jani & Solanki, 2014). κ-CG possesses satisfactory thermal stability (as compared to other polysaccharides) (Aleksandrova, Lesnichaya, Myachin, Sukhov & Trofimov, 2011), ability to different chemical functionalization (Sand, Mishra, Pandey, Mishra & Behari, 2012) and exhibits a number of membranotropic and anticoagulant (Yermak et al., 2012) properties. Therefore, the areas of κ-CG multi-purpose application are intensively expanded (for example, it is used as the gel-forming and binding agent, the component for tissue engineering, the interleukins inductor, the carrier for target therapy, etc.) (Li, Ni, Shao & Mao, 2014; Liu, Zhan, Wan, Wang & Wang, 2015; Lesnichaya, Aleksandrova, Sukhov, & Rokhin, 2013). Besides, earlier we showed that κ-CG could be efficiently employed as both reducing and stabilizing substance (i.e. without additional special reagents) for the green synthesis in water of the nanocomposites with silver nanoparticles possessing pronounced antimicrobial properties (Lesnichaya et al., 2010) and of the prebiotic nanocomposites with struvite nanoparticles (Lesnichaya et al., 2014). Thus, the combination of the availability of κ-CG with the widest spectrum of its biological activity allows easy to obtain nanocomposites that combine properties of metallic gold nanoparticles and biological and rheological properties of the κ-CG.

The present paper is aimed to one-step synthesis of gold-containing nanocomposites using κ-CG as a reducing and stabilizing matrix, as well as a further study of the structure and physical-chemical properties (including plasmonic-chiroptical phenomena imparted by plasmonic nanoparticles and natural chiral matrix).

2. Materials and methods

2.1. Materials

In this work, we used κ-CG (MW 1100 kDa) from CP Celko (Denmark), chloroauric acid Aldrich (USA), sodium hydroxide (NaOH) Reachim (Russia), ethyl alcohol (96%). All reagents were of chemical purity.

2.2. Synthesis of AuNPs-containing nanocomposites

An aqueous solution (5 ml) containing 0.46-1.43 g (1.36–4.23 mmol) $HAuCl_4$ was added to a solution of κ-CG (1 g) in distilled H_2O (60 ml) under stirring. The solution was kept at room temperature for 30 min, then pH was adjusted to pH = 10–11 by addition of 1N NaOH aqueous solution, and the solution was kept in a water bath at 70 °C for 15 min. The isolation of the target nanocomposites and their purification from impurities was performed by precipitation with a four-fold excess of EtOH, followed by repeated washing with ethanol and drying in air at room temperature.

2.3. The study of pH and temperature effects on the nanocomposites synthesis

An aqueous solution (5 ml) containing 0.46 g (1.36 mmol) $HAuCl_4$ was added to a solution of κ-CG (1 g) in distilled H_2O (60 ml) on stirring. The resulting solution (pH 2.22) was kept at room temperature for 30 min. To increase pH value up to 4.4, 6.6, and 10.8, aqueous solution of 1N NaOH was added to the initial reaction mixture. After that it was heated in a water bath at 70 °C until the appearance of characteristic features of AuNPs formation (the change to the violet color of reaction mixture because of the plasmon absorption of AuNPs). The optical absorption spectra of the reaction medium were recorded at 300–700 nm.

We studied also the reactions of nanocomposite synthesis at 60, 70, 80 and 90 °C (with fixed pH = 10.8).

2.4. Characterization and measurements

2.4.1. IR- and ^{13}C NMR spectroscopy of native κ-CG nanocomposites

IR spectra were recorded by a FT-IR (RAM II) Bruker Vertex 70 spectrometer in KBr pellets in the range 4000–400 cm^{-1}. ^{13}C NMR spectra of the solutions in D_2O (concentration was 2%) with added copper(2+) acetate as relaxant at 27 °C were measured by "Bruker DPX – 400" operating at 100.13 MHz. The chemical shifts of all carbon atoms are reported relative to DSS internal standard (d = 0.000 ppm) (Supporting Information).

IR (cm^{-1}): 3449 (ν O—H), 2963, 2823 (ν C—H), 1640, (ν O—H), 1255, 1381 (ester sulfate group), 934 (3,6-anhydrogalactose), 847 (galactose-4-sulfate).

^{13}C NMR of κ-CG (δ ppm): 104.7 (C-1 G4S),[1] 97.0 (C-1 DA),[2] 71.7 (C-2 G4S), 80.7 (C-3 G4S), 81.5 (C-3 DA), 76.0 (C-4 G4S), 80.6 (C-4 DA), 77.0 (C-5 G4S), 78.9 (C-5 DA), 63.5 (C-6 G4S).

2.4.2. Optical spectroscopy of AuNPs-containing nanocomposites

Optical absorption spectra of aqueous solutions of nanocomposites were recorded relative to H_2O on a Perkin Elmer Lambda 35 spectrophotometer in a quartz cell of $d = 1$ cm.

2.4.3. Elemental analysis (EA)

The gold content was determined by atomic absorption analysis using a Perkin Elmer Analyst 200 spectrometer. The sulfatation degree of κ-CG and its nanocomposites was determined by elemental analysis (according to the ratio of sulfur to carbon, hydrogen, and oxygen contents).

EA of κ-CG: C 33.1%, H 6.1%, S 6.8%, Na 3.36%, K 3.6%.

2.4.4. X-ray diffraction (XRD) analysis

X-ray diffraction study was carried out on a Bruker D8 ADVANCE X-ray diffractometer with Cu Kα – radiation mode Locked Coupled. The exposure time was 1 s for the phase analysis, and 3 s for the cell parameters and coherent lengths. Identification of crystalline phases was carried out by comparing the experimental interplanar distances and relative intensities with those of the reference. The cell parameters and the size of AuNPs were calculated by using a software package DIFFRACplus EVA 13.

[1] G4S – galactopyranose-4-sulphate units.
[2] DA- anhydrogalactopyranose units.

2.4.5. Transmission electron microscopy (TEM)

TEM measurements were performed by a Leo 906 E microscope operated at an accelerating voltage of 120 kV.

2.4.6. Dynamic light scattering (DLS) and static light scattering (SLS)

DLS and SLS measurements were performed simultaneously at 21 °C with Photocor_Complex (Photocor Instruments, Inc) equipped by a 20 mV He-Ne laser (λ = 632.8 nm). The incident light was attenuated 10 times by a filter. The scattering angle was changed in the range of $45^\circ \leq \theta \leq 135^\circ$. The homodyne signal was analyzed by a 288-channel multi-τ digital correlator (Photocor). The duration of a single measurement was typically about 100 s averaged over a minimum number of three runs. The autocorrelation function of the scattered light intensity, g^2, were analyzed by Alango DynaLS v2.0 software. At each concentration, the diffusion coefficient D was determined by extrapolation of the $D(q^2)$ dependence to $q^2 \to 0$, where q is the scattering vector. The extrapolation of D to infinite dilution gave D_0, from which the hydrodynamic radius R_h was calculated by using the Stokes-Einstein relation. The radius of gyration R_g was estimated by the double extrapolation of SLS data in the Zimm coordinates. Colloidal ζ-potentials were measured with Malvern Zeta-sizer at $\theta = 173^\circ$. The nanocomposites were dissolved in water cleaned through a syringe 0.2 μm filter. The cylindrical light scattering cells were cleaned by rinsing them in benzene, degassing and filling with a dust-free air. The concentration of nanocomposites in water was changed within the range of $0.04 \leq c \leq 0.34$ g/L.

2.4.7. Electron paramagnetic resonance (EPR)

EPR spectra were recorded with an X-band Bruker ELEXSYS E-580 spectrometer operating in the X-wave range of 9.7 GHz. The *g*-factor was measured with an accuracy of 0.0002 for narrow signals and 0.01 for wide signals. The EPR spectra were recorded at room temperature in quartz ampoules of 5 mm diameter. The following experimental conditions were used: the amplitude modulation of 1.0-3.0 G, the receiver gain of 60 dB, the time constant of 0.02 s, the conversion time of 0.06 s, the microwave power of 0.6325 mW. The narrow signals were accumulated by applying up to 100 scans. The size of nanoparticles was calculated in according to Kawabata's theory (Kawabata, 1970) using equation:

$$\Delta H = 1.78 \times 10^{11} \times (\Delta g)^2 \times d^2 \times \rho / V_F \times M,$$

where d – nanoparticles diameter, ρ – the metal density, V_F – the Fermi velocity, ΔH – the peak-to-peak linewidth, M – the atomic mass of the metal, Δg is the difference between the g value of the metal and the free-electron *g*-factor (2.0023), have been found by experiments.

2.4.8. The study of optical rotation of native κ-CG and its nanocomposites

Optical rotation as well as the optical rotation dispersion of κ-CG and its nanocomposites was studied with the help of polarimeter Polamat A (Carl Zeiss) at five wavelengths (366, 406, 436, 546, 578 nm), e.g. in the range corresponding to AuNPs plasmon resonance with maximum at 540 nm.

2.4.9. Measurement of aldehyde groups content

Aldehyde groups content in κ-CG and its nanocomposites was determined by the classical for carbohydrates quantitative Somogyi-Nelson method (Evenson, 2004).

2.4.10. Viscosity measurement

Intrinsic viscosities [η] of κ-CG and its nanocomposites were determined by viscometry using a VPZh type-2 capillar viscometer (the diameter of the capillar was 0.73 mm) and Huggins equation (Tager, 1978). The polymerization degree was determined by the Doublier's equation variant for polysaccharides $[\eta] = 0.168 DP^{0.98}$ (where DP is degree of polysaccharide polymerization) (Doublier, Launay & Cuvelier,1992). The calculations were carried out in the approximate equality to unknown Huggins viscometric constants for κ-CG, its nanocomposites, and to known Huggins constant for cellulose, a linear polysaccharide that is similar to the κ-CG.

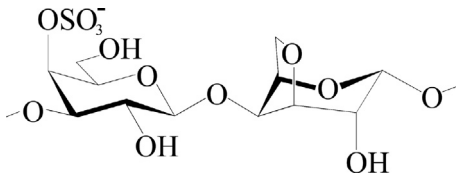

Scheme 1. The chemical structure of κ-carrageenan's unit.

2.4.11. Measurement of molar mass

Molar mass parameters of κ-CG and its nanocomposites were determined by means of high-pressure size-exclusion chromatography using an Agilent 1100/1260 liquid chromatograph with two tandem columns Ultrahydrogel Linear (Waters, USA), 300 mm long with inner diameter of 8 mm. The solutions were filtered through nylon filter Sartorius (Germany) with pores of 0.45 μm before injection. Concentration of the analyzed samples was of 1–4 mg/ml, the injected volume being of 100 μl. 0.1 mol/L aqueous solution of sodium nitrate was used as eluent, the flow rate being of 0.5 ml/min. The columns and detectors temperature was maintained at 40°C. Detection was performed in the three-channel mode using a differential refractometer (RID10A, Shimadzu), a multi-angle light scattering detector (Mini DAWN TriStar, Wyatt Technology Corporation, USA), and a spectrophotometer at 200–600 nm. The low-disperse polyethylene oxides and PSS pullulans (Germany) were used as standards for calibration. SEC results were processed taking advantage of the Astra 5.3.4.20 software.

3. Results

According to IR-, ^{13}C NMR spectroscopy (Van de Velde, Pereira & Rollema, 2004) and elemental analysis of used in this work κ-CG consist of regularly alternating residues of 3-O-substituted β-D-galactopyranose with the sulfate group substituent in the position 4 and the 4-O-substituted 3,6-anhydro-α-D- galactopyranose (Scheme 1).

The optical rotation of natural chiral polysaccharide κ-CG was determined $[\alpha]_{366}^{20} = +72$.

The degree of sulfatation is 6% and approximately corresponds to one sulfate group on the macromolecule κ-CG disaccharide unit. Its molecular weight is high (M_p 631.1 kDa, t_r 29.4 min, M_w 1009.0 kDa, M_n 564.7 kDa), α molecular mass distribution is broad, and the polydispersity index is (1.79). The only peak observed using a light scattering detector revealed a retention time (t_r 28.1 min). Hence, κ-CG molecules existed majorly in the non-aggregated state. It was experimentally established that at this molecular weight, aqueous solutions (1.6%) of k-carrageenan did not form gels at room temperature. Gel formation for this sample of carrageenan was observed only at 2% concentration in water. Besides, upon adding of $HAuCl_4$ to this solution, viscosity decrease of the solution was observed probably due to the significant lowering pH of the medium (up to 2.22). Such significant drop of pH facilitates deionization of functional sulphate groups with decreasing the charging of carrageenan macromolecule that suppresses gel formation.

The gold-containing nanocomposites (2.8–8.2% Au) were synthesized by reduction of $HAuCl_4$ in aqueous-alkaline medium at 60–90 °C in the presence of κ-CG. In this process, κ-CG acted

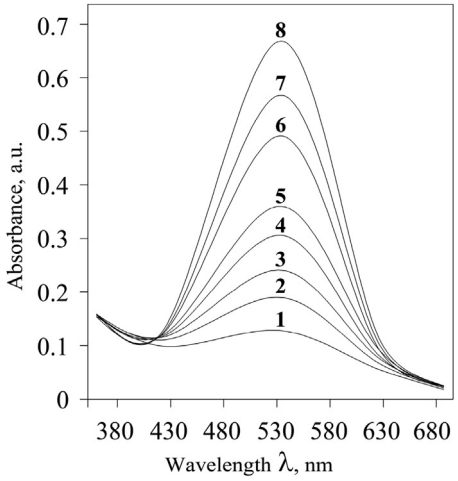

Fig. 1. Evolution of optical absorption spectrum of Au-containing nanocomposite AuNPs/κ-CG (2.8% of Au) in the course of synthesis at 70 °C.

as the reducing and stabilizing of gold nanoparticles. The formation of AuNPs was identified by changing of the reaction mixture color (from yellow to violet) and by the appearance of intensive absorption in the region 520–540 nm caused by AuNPs plasmon resonance. The content of Au in the nanocomposites was varied by changing the $HAuCl_4$/κ-CG ratio from 1.36 to 4.23 mmol of $HAuCl_4$ per 1 g of the polysaccharide. When the $HAuCl_4$/κ-CG ratio exceeded the limiting value (4.23 mmol of $HAuCl_4$ per 1 g of κ-CG), the formation of bulk metal gold took place that considerably decreased the target nanocomposite yield.

It is established that the forming of AuNPs most effectively proceeds when pH values exceed 10. The AuNPs formation is inhibited significantly when pH is 6–7 and is suppressed completely at pH values 4.4. At pH = 10, the optimal temperature range for the synthesis of nanocomposites is found to belong to the interval of 70–80 °C. At lower temperatures, the reaction slows down significantly. The reaction carried out at 90 °C is accompanied by a very rapid (<1 min) formation of plasmonic AuNPs followed by the bathochromic shift of their plasmonic absorption, obviously, due to AuNPs coalescence. Within next four minutes, the complete aggregation of AuNPs occurs, as observed by the disappearance of the violet color of the reaction medium and the precipitation of orange bulk metallic gold. Thus, the optimum conditions for the nanocomposites synthesis include pH values of more than 10 and temperature of 70–80 °C. Stable for a long time nanocomposites, involved in further study, were prepared in this optimal conditions.

The process of AuNPs formation in the κ-CG matrix was studied by using spectrometric monitoring of the plasmon absorption intensity in the initial stage of the AuNPs/κ-CG nanocomposite synthesis at the same $HAuCl_4$/κ-CG ratio (1.36 mmol/1 g) and at various temperatures (60–90 °C). For example, at 70 °C the increase in the reaction time from 0 to 8 min led to the appearance and growth of plasmon absorption intensity at λ 540 nm that indicated the precursor reduction and the generation of AuNPs in κ-CG matrix (Fig. 1).

We found that the formation of AuNPs in κ-CG matrix proceeds via two distinctly distinguishable stages. The first one, the induction period (which interval varied from 1 to 3 min, depending on the temperature), is characterized by the absence of plasmon optical absorption. At the second stage, the maximum of the plasmon resonance of AuNPs appears at 540 nm, and the color of solution changes from yellow to violet.

The optical absorption spectra of aqueous solutions of nanocomposites, containing different amount of gold, show one intensive

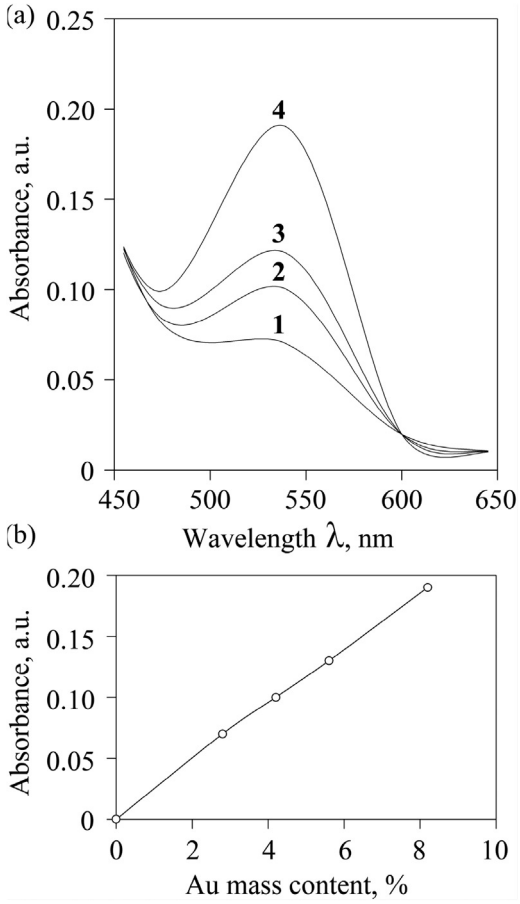

Fig. 2. (a) – Absorption spectra of water solutions of nanocomposites with the content of Au (w/w%): 2.8 (1); 4.2 (2); 5.6 (3); 8.2 (4) and (b) – linear dependence of optical absorption from content AuNPs.

symmetric maximum of plasmonic absorption at λ = 520–540 nm, characteristic of spherical AuNPs (Fig. 2).

The linear dependence of plasmonic absorption on Au content follows from inset of Fig. 2. This dependence can be used as the calibration curve for controlling AuNPs synthesis.

The polarimetric measurements show that the optical activity of nanocomposites drastically differs from that of pristine κ-CG. For example, the distinct S-shaped dependence of specific rotation on the light wavelength is observed in the region of plasmonic optical absorption of AuNPs (i.e. the Cotton negative effect on AuNPs plasmonic chromophore is observed), while the dispersion of optical rotation of the initial κ-CG is monotonous (Fig. 3).

The IR spectra (within their sensitivity) show that κ-CG does not undergo significant changes during the synthesis. For instance, the IR spectra of nanocomposites display the absorption bands assigned to antisymmetric and symmetric vibrations of the β-galactose cycle (910 and 771 cm^{-1}), stretching vibrations of equatorial sulfa-groups (1240 and 848 cm^{-1}) as well as hydroxyl groups (3560 and 3422 cm^{-1}). Nevertheless, the IR measurements allow the identification of the carbonyl and carboxyl groups vibrations in the 1700–1736 cm^{-1} range, arriving in the course of deep oxidation of κ-CG with gold precursor.

The quantitative Somogyi-Nelson method established the gradual accumulation of reducing aldehyde groups (from 0.04 to 6%) with gold content. This indicates the participation of κ-CG primary hydroxyl groups in the reduction of gold precursor. The degree of κ-CG sulphatation remains constant during the synthesis.

The viscometric molecular masses of nanocomposites decrease upon increasing gold content. Namely the following molecular

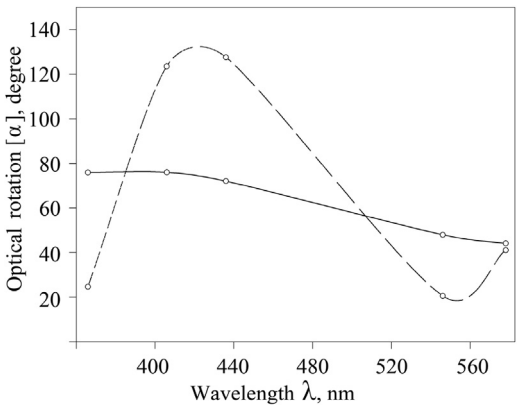

Fig. 3. The optical rotation dispersion of carrageenan – (1) and its AuNPs-containing nanocomposite (2.8% Au) – (2).

masses were observed: 1100, 900, 800, 600 kDa at 2.8, 4.2, 5.6, and 8.2 w/w% Au, respectively.

For the Au/κ-CG composite containing 5.6% of gold, the polysaccharide showed molecular mass of M_p 102.5 kDa (t_r 30 min) M_w 129.6 kDa, M_n 95.8 kDa, becoming highly degraded and more narrow disperse (1.35) as well. Light scattering detector registered the only peak with t_r 28.4 min. No peak of the aggregated macromolecules was observed; the calculated radius of κ-CG macromolecules in the Au/κ-CG composite was of 33 nm.

X-ray diffraction patterns of nanocomposites display the amorphous halo of κ-CG at $2\theta = 18–23$ as well as four intense reflections at $2\theta = 38.1$, 44.3, 64.3, and 77.6, related to (111) (200) (220), (311) planes of the face-centered cubic lattice of bulk gold crystals, respectively (Fig. 4).

The crystalline phase was identified by equality between the reference interplanar distances of bulk gold crystals ($a = 0.4078$ nm) with $a = 0.4073$ nm obtained experimentally for AuNPs. The average size of AuNPs, determined by the Debye-Scherrer formula, is 7.3 nm.

According to the microphotographs obtained by TEM, the nanocomposites contain almost spherical AuNPs of relatively narrow size distribution. The representative TEM photo is shown in Fig. 5 for the nanocomposite containing 2.8 w/w% of Au. The size of the majority (79%) of AuNPs belongs to the range of 6–12 nm, the size of the rest of AuNPs belongs to the range of 14–24 nm (Fig. 5). The average size of AuNPs is 11 nm, in good agreement with the results of X-ray diffraction analysis.

The representative EPR spectrum demonstrated in Fig. 6 shows that the nanocomposite contains wide signal which width is changing in the range of $595 \leq \Delta H \leq 750$ G, and the g-factor is changing from 2.12 to 2.045, respectively. There are also two narrow signals of lower g-factors (Fig. 6, inset): the width of the first is observed in the range of 7.1–8.4 G, the second in the range of 2.0–2.5 G. The size of AuNPs, determined by the Kawabata formula, is 7–8 nm. The EPR results for all nanocomposites are summarized in Table 1.

The colloid of the nanocomposite containing 4.2% Au was studied by SLS and DLS. The scattering from the virgin carrageenan solutions was negligibly small in comparison with the scattering resonantly enhanced by AuNPs plasmons, the same as for studied earlier nanocomposites with arabinogalactan (Gasilova et al., 2010). DLS exhibits bimodal R_h distributions with the maxima centered at $(R_h)_1 = 12.5 \pm 4$ and $(R_h)_2 = 150 \pm 10$ nm (Fig. 7). The radius of the minor component is slightly higher than that of AuNPs determined by TEM. Thus, we attribute the minor mode to the fraction of single AuNPs covered by κ-CG units. In accord with TEM microphotograph (Fig. 5) revealing several clusters of closely spaced AuNPs,

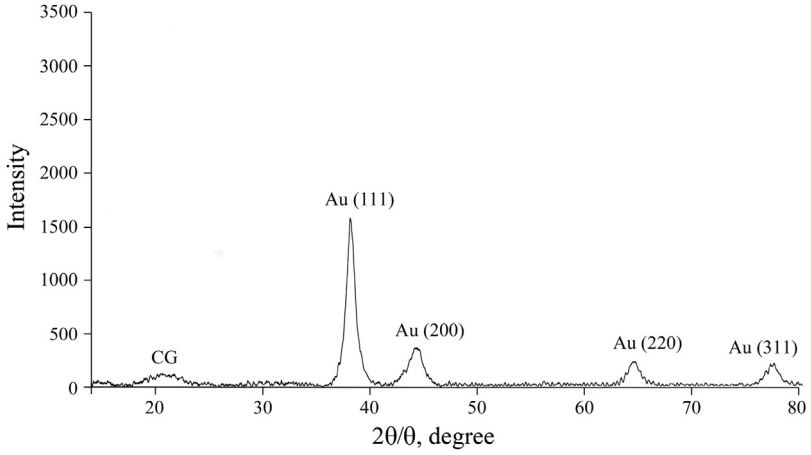

Fig. 4. X-ray diffraction pattern of κ-CG –based gold-containing nanocomposite (2.8% Au).

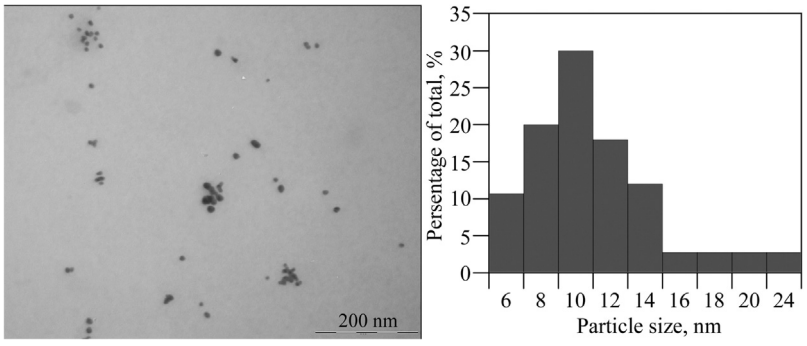

Fig. 5. TEM image of AuNPs in κ-CG matrix (the inset is the histogram of AuNPs size distribution).

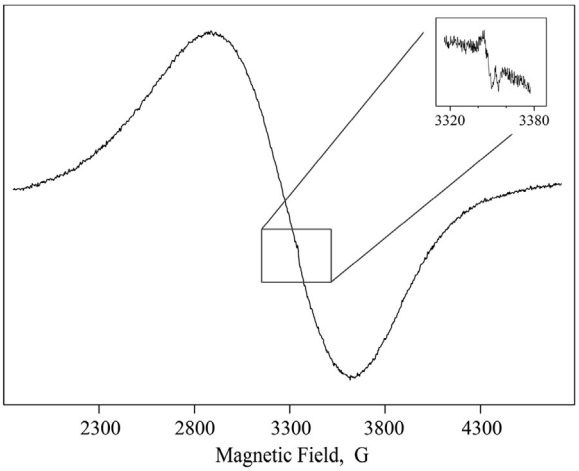

Fig. 6. The representative EPR spectrum of the nanocomposite containing 2.8% Au.

Table 1
The EPR characteristics of AuNPs/κ-CG-nanocomposites.

	wide signal		narrow signals	
Au, w/w%	Δ*H*, G	g-factor	Δ*H*, G	g-factor
2.8	595	2.12	8.2 2.0	2.0046 2.0007
4.2	750	2.08	7.5 2.1	2.0047 2.0006
5.6	740	2.05	8.4 2.5	2.0046 2.0005
8.2	603	2.045	7.1 2.0	2.0061 2.0009

we attribute the fraction of larger scatterers to the colloids containing nanoparticles ensembles (NPE). Although the scattering is governed by the coupled plasmons of NPE, the absorption spectrum (Fig. 2) is determined mainly by single AuNPs (the minor peak at 650 nm indicates, probably, the NPE contribution to the absorption). The scattering of light rather than the extinction spectroscopy is sensitive to NPE, as has been demonstrated, for example, in Ref (Sebba & Lazarides, 2008). The radii of gyration $R_g = 89 \pm 6$ nm were determined by the double extrapolation of SLS results plotted in the Zimm coordinates. The corresponding Zimm dependences on

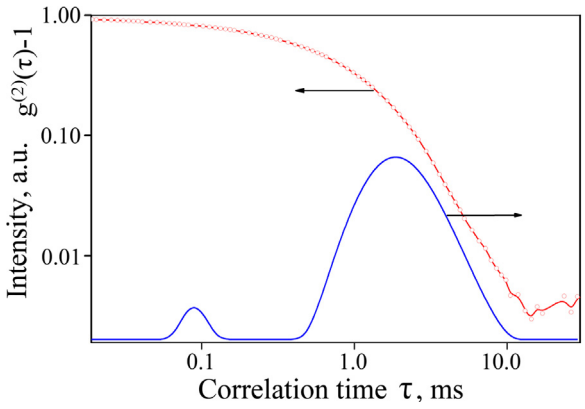

Fig. 7. Correlation function of scattered light intensity g^2 and the corresponding distribution of decay times τ (solid line). The scattering was determined at 90°. The corresponding colloids with one nanoparticle and NPE in the core are presented. (For interpretation of the references to colour in this figure legend, the reader is referred to the web version of this article.)

q^2 are linear, indicating that the contribution of the minor mode to the scattering intensity is negligible.

4. Discussion

One-step synthesis of water-soluble gold-containing nanocomposites was accomplished in aqueous medium using natural biocompatible polysaccharide κ-CG. The absence of any additional reducing and stabilizing agents evidences of this dual κ-CG role in the AuNPs synthesis. This obviates the necessity for application of potential environmentally unfriendly reducing agents and solvents for the synthesis of nanoparticles, and meets the main requirements of green synthesis. Similar to other polysaccharide-metal pairs (Grishchenko et al., 2006; Lesnichaya et al., 2010, 2011; Trofimov et al., 2007) the alkaline medium is important for effective reduction of gold-containing precursor with κ-CG (Scheme 2).

Thus, the additional reducing fragments of monosaccharides are produced due to the alkaline "peeling" of polysaccharide macromolecules (Lesnichaya, Aleksandrova, Sukhov & Rokhin, 2013). Also hydroxide anions bind the protons appearing in course of the redox reaction (Scheme 2) (Grishchenko et al., 2006; Lesnichaya et al., 2011).

It is important that even under highly alkaline conditions, the formation of precipitate $Au(OH)_3$ is slowed kinetically (Mironov,

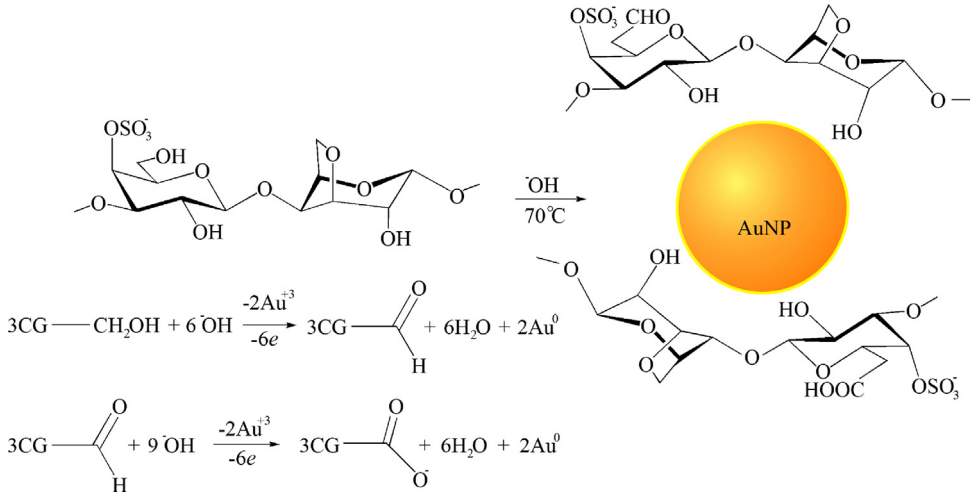

Scheme 2. Nanocomposites redox formation and main detected processes.

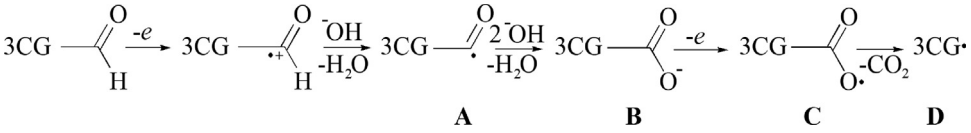

Scheme 3. Oxidative formation of paramagnetic centrum on κ-CG.

2005). Then the reaction mixture contains the oxidizing starting ion $[AuCl_4]^-$ and its hydrolyzed ions $[Au(OH)Cl_3]^-$, $[Au(OH)_2Cl_2]^-$, $[Au(OH)_3Cl]^-$, $[Au(OH)_4]^-$, capable of migration towards the reducing hydroxyl group and afterwards to the aldehyde group of polysaccharide (Scheme 2). The main contribution of the primary alcohol groups of κ-CG to gold reduction is confirmed by the fact that the final nanocomposite based on chiral polysaccharide retains its optical activity, while possible oxidation of chiral carbon at secondary alcohol groups would lead to the formation of achiral ketone groups and, consequently, to inevitably drop of optical activity.

Obviously, labile atoms of zero-valent gold, generated via the redox interaction, form primary small atomic gold clusters in the course of their diffusion movement. A peculiarity of their "nonplasmonic" structure is the absence of delocalized conducting electrons (Philip et al., 2012). Consequently, at this stage of the nanocomposites formation, the pronounced coloring of the reaction mixture is not observed because the plasmonic light absorption by metal nanoparticles is absent. This initial period of the nanocomposites synthesis can be considered as an induction period. Further on, small molecular clusters of gold grow either by addition of new zero-valent gold atoms or by coalescence. All these initial processes of gold clusters growth (proceeding before the formation of plasmonic nanoparticles) also belong to visible unobserved (no coloring) induction period of the nanobiocomposites formation. However, the subsequent growth of the nanoparticles up to the sizes sufficient for the emergence of the "metallic bond" phenomenon (appearance of loosely-bonded delocalized conductive electrons in the metal nanoparticles) will be accompanied by generation of characteristic plasmonic optical absorption of AuNPs (Kuzyk et al., 2012) which is observed after the induction period. Obviously, this stage involves the nucleation of new metal nanophase from the unstable atoms and atomical clusters of zero-valent gold formed at the first stage. Also, AuNPs of this phase are stabilized due to the absorption of κ-CG macromolecules on their surface to induce cooperative multi-linked coordination: electrostatic, Van der Waals and other interactions between the AuNPs surface and the biopolymer macromolecule (Scheme 2).

The observed decrease of the viscozimetric molecular mass of obtained nanocomposites is likely due to the degradation of κ-CG macromolecules via alkali peeling that proceeds sequentially, starting from the free terminal hemiacetal unit of polysaccharide (Lesnichaya et al., 2013).

The monotonic course of dispersion curve of the initial κ-CG optical rotation is caused by the absence of any chromophores of this natural enantiopure polysaccharide in the studied wavelengths region. However, the formation of AuNPs in the polysaccharide macromolecules results in appearance of such chromophore. It is a plasmonic excitation of conducting electrons of AuNPs with absorption maximum at 520–540 nm. The fact that the obtained nanocomposites show the pronounced Cotton effect in this region is indicates the immediate vicinity of the polysaccharide chiral centers to the surface of the plasmonic AuNPs. These κ-CG chiral centers are strongly affected by the electric field of intensive plasmonic vibrations generated by surface plasmonic resonance of AuNPs that leads to a specific excitation of the optical rotation in the plasmonic absorption region (Fig. 3). Alternatively, the chiroptical properties of κ-CG/AuNPs composites can be also explained by chiral arrangement of AuNPs templated by κ-CG's helices (Kuzyk et al., 2012). However, in this case "giant" values of Cotton effect should be observed (Droulias & Yannopapas, 2013), and in the present phenomenon it is likely that simple interaction of κ-CG chiral centers with the plasmon electric field on the AuNPs surface takes place.

The structure of colloidal aggregates was characterized by comparison of the magnitude of structure-sensitive ratio R_g/R_h with those determined for a set of models of different mass distribution, form, rigidity, solvent quality, etc (Burchard, 1999). In our case, $R_g/(R_h) = 0.6 \pm 0.1$ is lower than minimal $R_g/R_h = 0.78$ possible for the spherical scatterers with uniform density (Fig. 7).

This indicates that the colloidal mass is concentrated in the centre of colloidal aggregates. Such R_g/R_h have been observed in microgels and in the core-shell colloids with single AuNPs in the core, covered by the less dense polysaccharide's shell (Burchard, 1999; Gasilova & Aleksandrova, 2011). While R_h reflects the size of nondrained part of the whole colloid, R_g is determined solely by the size of AuNPs's ensemble within colloid. Therefore, the difference of $(R_h)^2 - R_g \approx 60$ nm corresponds to the thickness of κ-CG 's shell. High aggregation ability of κ-CG is probably responsible for the formation of AuNPs ensemble. Strongly negative ζ-potential of colloid (−78 mV) indicates the role of negatively charged $-SO_3^{2-}$ groups of κ-CG in the colloidal stabilization.

The analysis of literature data evidences that wide EPR signals of composites can arise either from conducting electron spin resonance (CESR), or from AuNPs ferromagnetism (Shin & Wu, 2010; Khutsishvili et al., 2014). As wide EPR signals are observed at ambient temperature, and the calculation with formula Kawabata taking into account the Δg for gold (Beuneu & Monod, 1978) gives AuNPs sizes of 7–8 nm that agrees with the average size of AuNPs in κ-CG matrix determined by XRD and TEM. Thus, the wide EPR line, obviously, should be attributed to the CESR of AuNPs. Although it is possible that both CESR and ferromagnetism contributions to the wide EPR signal (overlap of signals). Two narrow EPR signals most likely belong to the radical center of κ-CG macromolecules generated by the redox processes during the nanocomposites synthesis. The signal ($g \approx 2.0007$, $\Delta H \approx 2$ G) can be attributed to residual acyl radicals (Chatgilialoglu, Crich, Komatsu & Ryu, 1999; Conte, Miyamura, Kobayashi & Chechik, 2010) generated on κ-CG macromolecules (Scheme 3A). These radicals are the common intermediates in the aldehyde group oxidation (Conte et al., 2010; Gilbert et al., 1996). In our case, the enhanced formation of acyl radicals can be stimulated by AuNPs. Another symmetrical signal ($g \approx 2.005$, $\Delta H \approx 8$ G) probably belongs to residual free radicals of κ-CG, which arise from the deeper aldehyde oxidation via carboxylate groups (Scheme 3B) into carboxylate radicals (Scheme 3C) and their decarboxylated species (Scheme 3D).

The localization of the discussed radicals on κ-CG macromolecule contributes to their easy EPR detection. These usually highly reactive free radicals are sterically hindered on κ-CG matrix and therefore become stable analogically to other kinetically stable radicals. It should be noted that the EPR-detected B → C → D conversion (Scheme 3) represents the continuation of the main redox processes (Scheme 2). Essentially, these are the transformations of polysaccharide's gold-reducing carboxylate anions in the well-known Turkevich method of AuNPs synthesis (Turkevich, Stevenson & Hillier, 1951).

5. Conclusions

In summary, water-soluble gold-containing nanocomposites are synthesized in a one step in water by using readily available industrial natural biocompatible κ-CG. This polysaccharide acts simultaneously as a reducing agent of gold precursor ions and a stabilizer of AuNPs thus avoiding a need for additional reactants. Optimal parameters of the synthesis of the nanocomposites with tailored content of metal gold are determined. The structure of the novel composite nanomaterials was characterized by complementary physical and chemical methods both in solid state and aqueous solution. The nanobiocomposites retain main characteristics of the initial polysaccharide (degree of sulfatation, hydrophilicity, optical activity, etc.) that can ensure synergism of the properties of both gold nanoparticles and κ-carrageenan (chirality, biocompatibility, water-solubility, polyanionic, anticoagulant features, etc.), examples of which are the appearance of chiroplasmonic and magnetic properties of the nanocomposites. The novel gold-containing nanobiocomposites, synthesized by environmental-friendly method, are interesting in modern science, engineering and technology as perspective versatile materials (water-soluble optically active catalytic nanoreactors including their plasmon-enhanced variants, materials for coherent and nonlinear optics, plasmonics including chiroplasmonic phenomena, "giant" surface-enhanced spectroscopy kinds, analysis, detections, imaging and sensing, biomedical diagnostic and therapeutic agents, etc.).

Acknowledgments

Main results are obtained using the material and technical base of the Baikal analytical center for collective uses of Siberian Branch of the Russian Academy of Sciences with partial financial support from the state research task V.46.4.1 and the Russian Foundation for Basic Research (grant number 16-33-00623).

Appendix A. Supplementary data

Supplementary data associated with this article can be found, in the online version, at http://dx.doi.org/10.1016/j.carbpol.2017.07.040.

References

Aleksandrova, G. P., Lesnichaya, M. V., Myachin YuA. Sukhov, B. G., & Trofimov, B. A. (2011). Effect of silver nanoparticles on the thermal characteristics of nanocomposites of galactose-containing polysaccharides. *Doklady Chemistry*, *439*, 187–189.

Beuneu, F., & Monod, P. (1978). The elliott relation in pure metals. *Physical Reviews B*, *18*, 2422–2425.

Burchard, W. (1999). Solution properties of branched macromolecules. *Advanced Polimer Sciense*, *143*, 115–194.

Chatgilialoglu, C., Crich, D., Komatsu, M., & Ryu, I. (1999). Chemistry of acyl radicals. *Chemical Reviews*, *99*, 1991–2069.

Conte, M., Miyamura, H., Kobayashi, S., & Chechik, V. (2010). Enhanced acyl radical formation in the Au nanoparticle-catalysed aldehyde oxidation. *Chemical Communication*, *46*, 145–147.

Doublier, J. L., Launay, B., & Cuvelier, G. (1992). *Viscoelastic properties of foods*. New York, USA: Elsevier Applied Science.

Droulias, S., & Yannopapas, V. (2013). Broad-Band giant circular dichroism in metamaterials of twisted chains of metallic nanoparticles. *Journal Physical Chemistry C*, *117*, 1130–1135.

Evenson, M. A. (2004). The need for analytical chemistry in clinical chemistry training programs. *Journal Agricultural Food Chemistry*, *52*, 8039–8045.

Gasilova, E. R., & Aleksandrova, G. P. (2011). Influence of gold content on colloidal structure of gold nanoparticles capped with arabinogalactan. *Journal Physical Chemistry C*, *115*, 24627–24635.

Gasilova, E. R., Toropova, A. A., Bushin, S. V., Khripunov, A. K., Grischenko, L. A., & Aleksandrova, G. P. (2010). Light scattering from aqueous solutions of colloid metal nanoparticles stabilized by natural polysaccharide arabinogalactan. *Journal Physical Chemistry B*, *114*, 4204–4212.

Gilbert, B. C., Hodges, G. R., Lindsay-Smith, J. R., MacFaul, P., & Taylor, P. (1996). Photo-decarboxylation of substituted alkylcarboxylic acids brought about by visible light and iron(III) tetra(2-*N*-methylpyridyl)-Porphyrin in aqueous solution. *Journal of the Chemical Society*, *2*, 519–524.

Grishchenko, L. A., Medvedeva, S. A., Aleksandrova, G. P., Feoktistova, L. P., Sapozhnikov, A. N., Sukhov, B. G., et al. (2006). Redox reactions of arabinogalactan with silver ions and formation of nanocomposites. *Russian Journal General Chemistry*, *76*, 1111–1116.

Kale, M. J., Avanesian, T., & Christopher, P. (2014). Direct photocatalysis by plasmonic nanostructures. *ACS Catalysis*, *4*, 116–128.

Kawabata, A. (1970). Electronic properties of fine metallic particles. III. E.S.R absorption line shape. *Journal Physical Society Japan*, *29*, 902–911.

Khutsishvili, S., Vakul'skaya, T., Kuznetsova, N., Ermakova, T., Pozdnyakov, A., & Prozorova, G. (2014). Formation of stable paramagnetic nanocomposites containing zero-valence silver and copper in polymeric matrix. *Journal Physical Chemistry C*, *118*, 19338–19344.

Kim, Y., Yeom, B., Arteaga, O., Jo, Y., Lee, S., Kim, J., et al. (2016). Reconfigurable chiroptical nanocomposites with chirality transfer from the macro- to the nanoscale. *Nature Materials*, *15*, 461–468.

Kuzyk, A., Schreiber, R., Fan, Z., Pardatscher, G., Roller, E.-M., Högele, A., et al. (2012). DNA-based self-assembly of chiral plasmonic nanostructures with tailored optical response. *Nature*, *483*, 311–314.

Lan, X., & Wang, Q. (2016). Self-assembly of chiral plasmonic nanostructures. *Advanced Materials*, http://dx.doi.org/10.1002/adma.201600697

Lesnichaya, M. V., Aleksandrova, G. P., Feoktistova, L. P., Sapozhnikov, A. N., Fadeeva, T. V., Sukhov, B. G., et al. (2010). Silver-containing nanocomposites based on galactomannan and carrageenan: Synthesis, structure, and antimicrobial properties. *Russian Chemistry Bulletin*, *59*, 2323–2328.

Lesnichaya, M. V., Aleksandrova, G. P., Feoktistova, L. P., Sapozhnikov, A. N., Sukhov, B. G., & Trofimov, B. A. (2011). Formation kinetics of gold nanoparticles in the galactomannan polysaccharide matrix. *Doklady Chemistry*, *440*, 282–285.

Lesnichaya, M. V., Aleksandrova, G. P., Sukhov, B. G., & Rokhin, A. V. (2013). Molecular-weight characteristics of galactomannan and carrageenan. *Chemistry Nature Compound*, *49*, 405–409.

Lesnichaya, M. V., Sukhov, B. G., Sapozhnikov, A. N., Safronova, L. A., Evseenko, O. V., Ilyash, V. M., et al. (2014). New nanobiocomposites of ammonium magnesium phosphate and carrageenan as efficient prebiotics. *Doklady Chemistry*, *457*, 144–147.

Li, L., Ni, R., Shao, Y., & Mao, S. (2014). Carrageenan and its applications in drug delivery. *Carbohydrate Polymers*, *103*, 1–11.

Liu, J., Zhan, X., Wan, J., Wang, Y., & Wang, C. (2015). Review for carrageenan-based pharmaceutical biomaterials: Favourable physical features *versus* adverse biological effects. *Carbohydrate Polymers*, *121*, 27–36.

Marradi, M., Chiodo, F., García, I., & Penadés, S. (2013). Glyconanoparticles as multifunctional and multimodal carbohydrate systems. *Chemical Society Reviews*, *42*, 4728–4745.

Mironov, I. V. (2005). Properties of gold (III) hydroxide and aquahydroxogold (III) complexes in aqueous solution. *Russian Journal Inorganic Chemistry*, *50*, 1115–1120.

Mittal, A. K., Chisti, Y., & Banerjee, U. (2013). Synthesis of metallic nanoparticles using plant extracts. *Biotechnology Advanced*, *31*, 346–356.

Noruzi, M. (2015). Biosynthesis of gold nanoparticles using plant extracts. *Bioprocess Biosystems Engineering*, *38*, 1–14.

Philip, R., Chantharasupawong, P., Qian, H., Jin, R., & Thomas, J. (2012). Evolution of nonlinear optical properties: From gold atomic clusters to plasmonic nanocrystals. *Nano Letters*, *12*, 4661–4667.

Prajapati, V. D., Maheriya, P. M., Jani, G. K., & Solanki, H. K. (2014). Carrageenan: A natural seaweed polysaccharide and its applications. *Carbohydrate Polymers*, *105*, 97–112.

Sand, A., Mishra, D. K., Pandey, V. S., Mishra, M. M., & Behari, K. (2012). Synthesis of graft copolymer (CgOH-g-AGA): Physicochemical properties, characterization and application. *Carbohydrate Polymers*, *90*, 901–907.

Sebba, D. S., & Lazarides, A. A. (2008). Robust detection of plasmon coupling in core-satellite nanoassemblies linked by DNA. *Journal Physical Chemistry C*, *112*, 18331–18339.

Shin, P.-H., & Wu, S. Y. (2010). Magnetic anisotropic energy gap and strain effect in Au nanoparticles. *Nanoscale Research Letters*, *5*, 25–30.

Shurygina, I. A., Sukhov, B. G., Fadeeva, T. V., Umanets, V. A., Shurygin, M. G., Ganenko, T. V., et al. (2011). Bactericidal action of Ag(0)- antithrombotic sulfated arabinogalactan nanocomposite: Coevolution of initial nanocomposite and living microbial cell to a novel non-living nanocomposite. *Nanomedicine: NBM*, *7*, 827–833.

Tager, A. A. (1978). *Physicochemistry of polymers*; Khimiya, Moscow, Russia.

Trofimov, B. A., Sukhov, B. G., Aleksandrova, G. P., Medvedeva, S. A., Grishchenko, L. A., Mal'kina, A. G., et al. (2003). Nanocomposites with magnetic, optical, catalytic, and biologically active properties based on arabinogalactan. *Doklady Chemistry*, *393*, 287–288.

Trofimov, B. A., Sukhov, B. G., Nosyreva, V. V., Mal'kina, A. G., Aleksandrova, G. P., & Grishchenko, L. A. (2007). Pd(0)-arabinogalactan nanocomposites as catalysts for dimerization of acetylenic compounds. *Doklady Chemistry*, *417*, 261–263.

Turkevich, J., Stevenson, P. C., & Hillier, J. (1951). A study of the nucleation and growth processes in the synthesis of colloidal gold. *Discussions of the Faraday Society*, *11*, 55–75.

Van de Velde, F., Pereira, L., & Rollema, H. (2004). The revised NMR chemical shift data of carrageenans. *Carbohydrate Research*, *339*, 2309–2313.

Yamada, M., Foot, M., & Prow, T. (2015). Therapeutic gold, silver, and platinum nanoparticles. *WIREs Nanomedicine and Nanobiotechnology*, *7*, 428–445.
Yasukawa, T., Miyamura, H., & Kobayashi, S. (2014). Chiral metal nanoparticle-catalyzed asymmetric CC bond formation reactions. *Chemical Society Reviews*, *43*, 1450–1461.
Yermak, I. M., Barabanova, A. O., Aminin, D. L., Davydova, V. N., Sokolova, E. V., Solov'eva, T. F., et al. (2012). Effects of structural peculiarities of carrageenans on their immunomodulatory and anticoagulant activities. *Carbohydrate Polymers*, *87*, 713–720.
Zhao, P., Li, N., & Astruc, D. (2013). State of the art in the synthesis of gold nanoparticles. *Coordination Chemistry Reviews*, *257*, 638–665.
Zheng, Y., Monty, J., & Linhardt, R. (2015). Polysaccharide-based nanocomposites and their applications. *Carbohydrate Research*, *405*, 23–32.